The Putative "Nucleation Site" in Human H-Chain Ferritin Is Not Required for Mineralization of the Iron Core†

Fadi Bou-Abdallah,‡ Giorgio Biasiotto,§ Paolo Arosio,§ and N. Dennis Chasteen*,‡

Department of Chemistry, University of New Hampshire, Durham, New Hampshire 03824, and Chemistry Section, Faculty of Medicine, University of Brescia, 25123 Brescia, Italy

Received January 15, 2004; Revised Manuscript Received February 11, 2004

ABSTRACT: It is widely believed that the putative nucleation site (Glu61, Glu64, and Glu67) in mammalian H-chain ferritin plays an important role in mineral core formation in this protein. Studies of nucleation site variant A2 (E61A/E64A/E67A) of H-chain ferritin have traditionally shown impaired iron oxidation activity and mineralization. However, recent measurements have suggested that the previously observed impairment may be due to disruption of the ferroxidase site of the protein since Glu61 is a shared ligand of the ferroxidase and nucleation sites of the protein. This study employed a new nucleation site variant A1 (E64A/E67A) which retains the ferroxidase site ligand Glu61. The data (O_2 uptake, iron binding, and conventional and stopped-flow kinetics measurements) show that variant A1 retains a completely functional ferroxidase site and has iron oxidation and mineralization properties similar to those of the wild-type human H-chain protein. Thus, in contrast to previously published literature, this study demonstrates that the putative "nucleation site" does not play an important role in iron uptake or mineralization in H-chain ferritin.

Ferritins are ubiquitous iron biomineralizing proteins that play an important role in iron storage and detoxification (*1*, *2*). Mammalian ferritins are heteropolymers composed of 24 subunits of two types designated H for heavy ($M_r \sim 21\,000$ Da) and L for light ($M_r \sim 20\,000$ Da). The subunits assemble to form a central cavity capable of accommodating as many as 4500 iron atoms in the form of a mineral iron core that resembles the mineral ferrihydrite, $5Fe_2O_3 \cdot 9H_2O$ (*3*).

The H-chain ferritin (HuHF)[1] has a diiron ferroxidase center capable of rapidly oxidizing Fe(II) to Fe(III), whereas L-chain ferritin (HuLF) lacks such a center but still incorporates iron, albeit at a reduced rate compared to that of the homopolymer H-chain (*1*, *4*−*7*). As shown in Figure 1, the ferroxidase center in HuHF involves two binding sites, A and B, with site A consisting of coordinating residues Glu27, His65, Glu62, and Gln141 and site B consisting of coordinating residues Glu62, Glu61, and Glu107, with residue Glu62 bridging the two sites.

The differences in the iron oxidation activities between HuHF and HuLF are mainly due to the specific amino acid residues that form the ferroxidase center in HuHF but are absent in HuLF (Figure 1). The amino acid residues constituting the ferroxidase site are highly conserved among

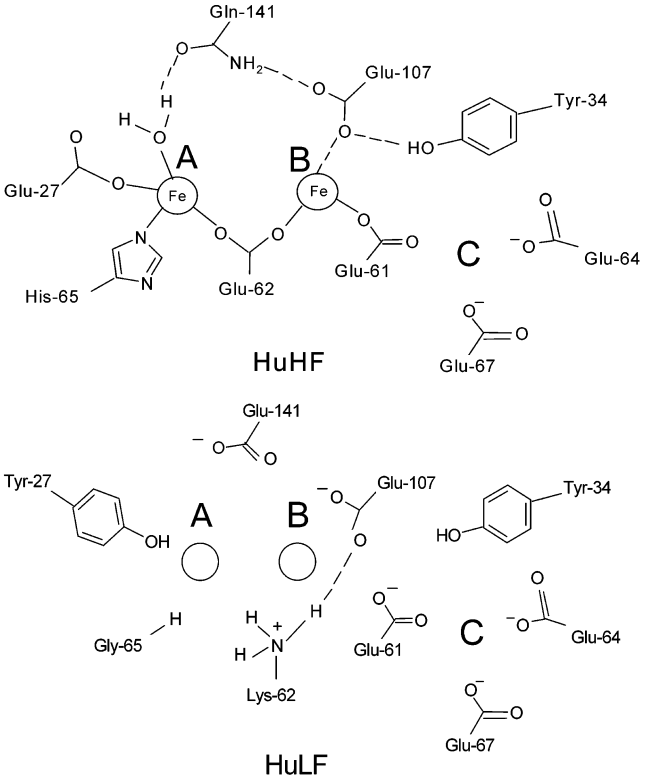

FIGURE 1: Schematic diagram of the ferroxidase center in human H-chain ferritin and the corresponding residues in human L-chain ferritin. The A- and B-sites of the dinuclear center and the putative nucleation C-site are denoted. H-Chain numbering of amino acid residues is employed throughout the paper.

† This work was supported by Grant R37 GM20194 from the National Institute of General Medical Sciences (N.D.C.) and by Grant MIUR-FIRB and Cofin-02 (P.A.).

* To whom correspondence should be addressed: Department of Chemistry, Parsons Hall, University of New Hampshire, Durham, NH 03824. Phone: (603) 862-2520. Fax: (603) 862-4278. E-mail: ndc@cisunix.unh.edu.

‡ University of New Hampshire.

§ University of Brescia.

[1] Abbreviations: HuHF and HuLF, recombinant human H- and L-chain ferritins, respectively; A2, nucleation site residue (E61A/E64A/E67A); A1, new engineered nucleation site residue (E64A/E67A); EcBFR, *Escherichia coli* bacterioferritin; EcFtnA, *E. coli* bacterial ferritin type A; HoSF, horse spleen ferritin; Mes, 2-(*N*-morpholino)-ethanesulfonic acid; Mops, 3-(*N*-morpholino)propanesulfonic acid; Hepes, *N*-(2-hydroxyethyl)piperazine-*N*′-2-ethanesulfonic acid.

10.1021/bi0498813 CCC: $27.50
Published on Web 03/18/2004

ferritins from different species (*2*). A cluster of negatively charged residues on the cavity surface (Glu107, Glu57, Glu60, Glu61, Glu64, and Glu67) is thought to be responsible for the slow incorporation of iron in the L-chain *in vitro* (*1*, *5*−*8*). In L-chain ferritin, residue Glu62 is substituted with Lys which forms a salt bridge with its neighbor, Glu107 (*9*; Figure 1). The higher stability of L-chain ferritin is thought to be due in part to the presence of this salt bridge conferring more resistance to denaturation in HuLF than in any of the recombinant H-chain ferritins (*10*). The distribution and composition of ferritins in mammals are organ-dependent, emphasizing the importance of the L-chain in mineral core nucleation and the H-chain in rapid iron oxidation and detoxification. For instance, ferritins in iron storage organs such as liver and spleen are rich in L-chains, whereas those from heart and erythrocytes are rich in H-chains (*2*).

Iron oxidation and mineral core formation in ferritins have been widely studied *in vitro*. Recently, a detailed study of the mechanism of iron deposition in mammalian ferritins revealed at least three different pathways for mineral core formation, a protein-catalyzed ferroxidation reaction, a mineral surface reaction, and an Fe(II) + H_2O_2 detoxification reaction (*4*). The ferroxidation reaction involves the ferroxidase center of the protein which is responsible for the rapid oxidation of Fe(II) to Fe(III) through the formation of a μ-1,2-peroxodiiron(III) complex within the first 100 ms of the reaction. This peroxo intermediate subsequently decays within 10−15 s to form a μ-1,2-oxo/hydroxodiiron(III) complex(es) which ultimately vacates the ferroxidase center of the protein to regenerate its ferroxidase activity. Once a sizable core is formed inside the protein cavity, the mineral surface autoxidation reaction becomes the primary pathway for further iron oxidation (*4*). The detoxification reaction involves the pairwise oxidation of Fe(II) by H_2O_2 under moderate iron flux into the protein (100−500 Fe protein) and further contributes to the building of the mineral core.

Earlier studies have suggested or assumed that the cluster of Glu residues (Glu61, Glu64, and Glu67) on the inner surface of the H-subunit are important for mineral core nucleation (*6*, *7*, *11*−*13*) and that residue Glu61 can occupy two positions, one directed toward the B-site of the ferroxidase center and the other toward the putative nucleation C-site (Figure 1). An attractive possibility was that Glu61 acts as a shuttle, facilitating migration of iron from the ferroxidase site to the nucleation site where mineral core nucleation then ensues (*11*). Consistent with this idea, early studies with nucleation site variant A2 (E61A/E64A/E67A) showed impairment of core formation (*7*, *12*). However, recent Fe(III) binding and kinetic measurements on nucleation site variant A2 (*4*) showed reduced iron binding stoichiometry (24 Fe protein) compared to that of the wild-type protein (48 Fe protein) and much lower ferroxidase activity, in accord with earlier work (*5*), raising concerns about the integrity of the ferroxidase site of this variant. Since Glu61 is a ligand shared between the putative nucleation and ferroxidation sites (Figure 1), kinetic data on variant A2 are confounded by structural changes in both sites, making it impossible to draw definitive conclusions about the role of the nucleation C-site itself in mineralization of the iron core.

In the paper presented here, we have reinvestigated the role of the "nucleation site" residues in mineral core formation in ferritin using a newly engineered variant, A1, in which only two residues of the putative nucleation site (Glu64 and Glu67) have been mutated to Ala, thus preserving the functionality of the ferroxidase center. Both proteins, variant A1 and HuHF, exhibit similar stopped-flow kinetic profiles for formation and decay of the peroxodiiron(III) complex, an indication of fully intact and functional ferroxidase centers. The kinetics of core formation in variant A1 and the wild-type homopolymer HuHF are essentially identical, even with a high flux of iron (300−1000 Fe atoms/protein) into the protein. Similarly, both proteins exhibit binding stoichiometries of 48 Fe(III) protein and iron oxidation stoichiometries of 2.1 ± 0.2 Fe(II) O_2 [≤48 Fe(II) protein], increasing to 3.5 ± 0.1 Fe(II) O_2 [500−1000 Fe(II) protein]. Thus, this work does not support a role for residues Glu64 and Glu67 in iron uptake or mineralization by H-chain ferritins.

MATERIALS AND METHODS

Preparation and purification of HuHF and A1 were performed as previously described (*14*). The two recombinant proteins were subjected to two anaerobic reductions using 55 and 5 mM sodium dithionite in 50 mM Mes (pH 6.0) for 3 days each followed by 2 days of anaerobic dialysis against 1 mM 2,2′-bipyridyl and 50 mM Mes (pH 6.0) (*4*). The resulting solution was dialyzed against the working buffer used in the experiments. The apoprotein concentrations were determined spectrophotometrically using a molar absorptivity of 23 000 cm^{-1} M^{-1} at 280 nm (*4*). All chemicals were reagent-grade and used without further purification. Mops and Hepes buffers were purchased from Research Organics (Cleveland, OH), $FeSO_4 \cdot 7H_2O$ was from J. T. Baker, and sodium dithionite, $Na_2S_2O_4$, and 2,2′-bipyridyl were from Aldrich. Fe(II) stock solutions were freshly prepared immediately before each experiment in a dilute HCl solution at pH 3.0. The oximetry experiments were performed with an OM-4 oxygen meter (Microelectrodes, Inc., Bedford, NH) equipped with an MI-730 micro-oxygen electrode. The electrode oximetry apparatus and standardization reactions have been described in detail elsewhere (*15*). The fast kinetics experiments were conducted with a pneumatic drive Hi-Tech SFA-20M stopped-flow accessory on a J&M GmbH Tidas diode array spectrophotometer. The 650 nm absorbance of the peroxodiiron(III) complex formed after mixing the apoprotein with Fe(II) in the presence of oxygen was monitored every 2.5 ms following the first 8 ms of the reaction (which is the approximate dead time of the stopped-flow/diode array apparatus). Conventional ultraviolet visible spectroscopy was performed on a Varian Cary 50 spectrophotometer. The spectrophotometric data were further analyzed with Origin version 7.0 (OriginLab Corp.).

RESULTS

Stoichiometry of Oxygen Consumption in Variant A1. Figure 2 shows the oxygen uptake curves for consecutive additions of 48 Fe(II) protein to variant A1 in 0.1 M Mops (pH 7.0). The inset of Figure 2 indicates the dependence of the Fe(II)/O_2 stoichiometric ratio, measured after each Fe(II) addition, on the total amount of iron added. The oxidation of approximately 2 Fe(II) per O_2 for the first 48 Fe(II) added implies that hydrogen peroxide is a product in this reaction, in accord with previous findings with HuHF and other

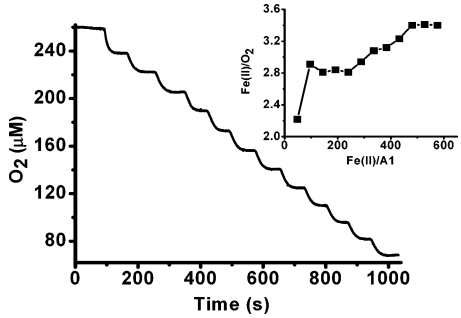

FIGURE 2: Oxygen consumption vs time for Fe(II) oxidation in A1 after 12 consecutive additions of 48 Fe(II) atoms/protein. The inset shows the Fe(II)/O_2 stoichiometry vs Fe(II)/A1 for the 12 sequential additions of 48 Fe(II) atoms/A1. Conditions: 1 μM protein, 48 μM Fe(II) per addition, 0.1 M Mops, pH 7.0, and 25 °C.

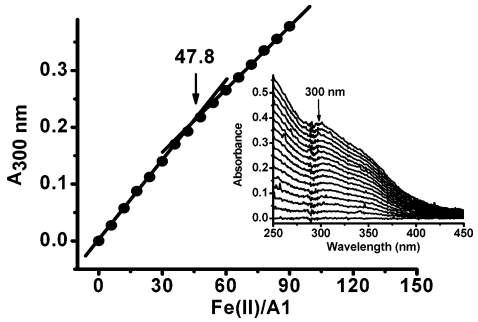

FIGURE 3: Aerobic spectrophotometric titration of variant A1 (E64A/E67A) with Fe(II). The inset shows the titration curve. Conditions: 1.5 μM protein, 9 μM Fe(II) [6 Fe(II) atoms per shell per injection], 0.1 M Mops, pH 7.0, and 25 °C.

ferritins (*15*−*18*). The Fe(II)/O_2 stoichiometry markedly increases from ∼2 Fe(II) O_2 for the first 48 Fe(II) protein to ∼2.8 Fe(II) O_2 for the second addition of 48 Fe(II) protein and reaches a plateau at this value until ∼250 Fe(II) protein have been added (Figure 2, inset). The stoichiometry then climbs to ∼3.5 for the 10th through 12th additions. Similar behavior was previously observed with HuHF and was attributed to the mineral surface reaction becoming the primary pathway for iron oxidation once a mineral core of ∼200−250 Fe has been formed inside the protein cavity (*4*). In a different set of experiments, the Fe(II)/O_2 stoichiometry did not increase beyond ∼3.5 to the theoretical value of 4.0 even when varying amounts of Fe(II) [500−1000 Fe(II) A1] were added to the apoprotein in a single addition, indicating that some of the O_2 was not completely reduced to H_2O. Moreover, the lack of precipitation up to 2050 Fe(II) protein, the largest amount of iron attempted, indicated that the iron remained associated with the protein in solution.

Spectrophotometric Titration of Variant A1 with Fe(II). To determine the Fe(III)/protein binding stoichiometry when Fe(II) is oxidized by O_2 in variant A1, a careful UV spectrometric titration was carried out (Figure 3). Fe(II) was added in small increments to the protein solution in the presence of oxygen, and the increase in absorbance at 300 nm was monitored. Figure 3 shows a discontinuity in the absorbance when ∼48 Fe(II) protein are added, consistent with iron binding and oxidation at the ferroxidase site of the protein [2 Fe(III) ferroxidase site], as previously found for HuHF (*15*). The molar absorptivity of the observed oxidation product at the ferroxidase site of variant A1 is 3125 M^{-1} cm^{-1} per iron at 300 nm, which is similar to the reported

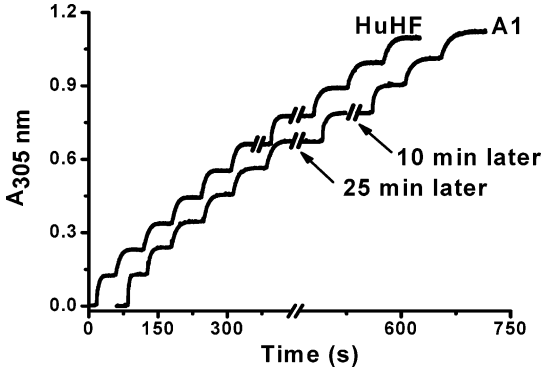

FIGURE 4: Kinetic curves following multiple additions of 48 Fe(II) atoms/shell to HuHF and variant A1. For clarity, the curve for variant A1 is offset on the time axis. Conditions: 1 μM protein, 48 μM Fe(II) per addition, 0.1 M Hepes, pH 7.0, and 25 °C. Additions of 48 Fe(II) atoms/shell were made as follows: immediate sequential additions for curves 1−6, 25 min later for curve 7, 10 min later for curve 8, and immediate sequential additions for curves 9 and 10.

values for other ferritins, including HuHF, HoSF, and EcBFR (*15*−*17*, *19*). This absorption band has been previously assigned to a ligand−metal charge transfer transition of μ-oxo-bridged iron(III) complexes in these proteins (*15*−*18*). Thus, we postulate that the oxidized/hydrolyzed iron species at the ferroxidase site of variant A1 is a μ-oxo/hydroxo-bridged diiron(III) complex. Similarly, when large amounts of Fe(II) are added to the apoprotein [i.e., 1000 Fe(II) shell], the corresponding molar absorptivity of the μ-oxo/hydroxo-bridged iron(III) clusters that are formed is 2540 M^{-1} cm^{-1} per iron, which is similar to values previously reported for other ferritins (*4*, *15*−*17*, *19*).

Kinetics of Fe(II) Oxidation and Mineralization in Variant A1. Spectrophotometric kinetics measurements were conducted to evaluate the importance of Glu64 and Glu67 in the formation of the mineral core at low and high iron loadings of variant A1. Figure 4 shows the increase in absorbance at 305 nm after multiple additions of 48 Fe(II) were made to the same protein sample of A1 or HuHF. Similar progressively slower initial rates of iron oxidation are observed in both proteins following the six sequential additions of 48 Fe(II) shell (Table 1). However, addition of another 48 Fe(II) shell 25 and 10 min later for the seventh and eighth injections, respectively, to the same protein sample indicates that, upon standing, variant A1 regenerated ∼85% of its ferroxidase activity (0.051 s^{-1} vs 0.060 s^{-1}) compared to only ∼45% for HuHF (0.023 s^{-1} vs 0.050 s^{-1}) (Table 1). This result suggests that iron turnover in variant A1, as reflected in the kinetic rates, is somewhat faster than in HuHF. In a different set of experiments, neither HuHF or A1 was able to fully regenerate its initial ferroxidase activity even after 15 h, both proteins achieving only 85% of the rates observed for the addition of the first 48 Fe(II) protein (data not shown).

To determine whether the putative nucleation site is required to process a large amount of iron when presented to the protein, 1000 Fe(II) shell were added to both variant A1 and HuHF and the kinetic curves for mineral core formation followed at 305 nm (Figure 5A). In another experiment, 300 Fe(II) shell were added to both proteins followed by another 300 Fe(II) shell 30 min later (Figure 5B). Both proteins process iron equally well, indicating

Table 1: Initial Rates of Fe(II) Oxidation Following the Additions of 48 Fe(II) Atoms/Protein at the Indicated Times

	injection 1[a]	injection 2[a]	injection 3[a]	injection 4[a]	injection 5[a]	injection 6[a]	injection 7[a]	injection 8[a]	injection 9[a]	injection 10[a]
Fe(II)/shell	48	48	48	48	48	48	48 (25 min later)	48 (10 min later)	48	48
initial rate of Fe(II) oxidation in HuHF	0.050 ± 0.002	0.022 ± 0.006	0.014 ± 0.005	0.014 ± 0.004	0.013 ± 0.003	0.009 ± 0.002	0.023 ± 0.009	0.024 ± 0.004	0.016 ± 0.004	0.018 ± 0.006
initial rate of Fe(II) oxidation in variant A1	0.061 ± 0.005	0.019 ± 0.003	0.013 ± 0.001	0.013 ± 0.001	0.012 ± 0.001	0.01 ± 0.001	0.051 ± 0.003	0.043 ± 0.007	0.015 ± 0.001	0.015 ± 0.001

[a] Injections 1−6, 9, and 10 were made sequentially; injections 7 and 8 were made 25 and 10 min after the sixth and the seventh injections, respectively. Standard errors from replicate determinations are given.

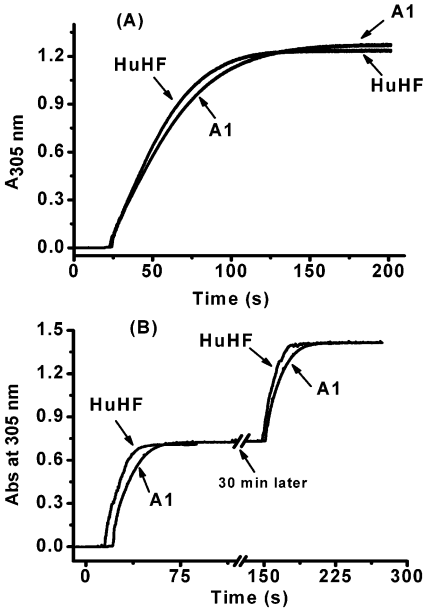

FIGURE 5: Kinetic curves for the formation of the Fe(III) core in HuHF and variant A1 following (A) addition of 1000 Fe(II) atoms/shell and (B) two additions of 300 Fe(II) atoms/shell spaced at 30 min. Conditions: (A) 0.5 μM protein and 500 μM Fe(II) and (B) 1.0 μM protein, 300 μM Fe(II), 0.1 M Mops, pH 7.0, and 25 °C.

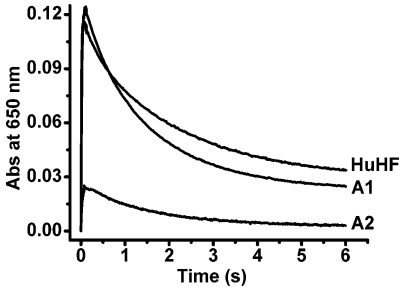

FIGURE 6: Stopped-flow kinetics measurements of the formation and decay of the μ-peroxodiiron(III) complex in HuHF and variants A1 and A2 at 650 nm. Conditions: 5 μM protein in 21% O_2, 0.24 mM $FeSO_4$ (pH 3.0), 50 mM Mops, pH 7.0, and 25 °C. The reported values are final concentrations after the two reagents were mixed in the stopped-flow cell.

that Glu64 and Glu67 are not critical for mineral core formation.

Formation of a Peroxodiiron(III) Complex in Variant A1. Diode array stopped-flow spectrophotometry measurements of the formation of the μ-peroxodiiron(III) complex (λ_{max} = 650 nm, blue intermediate) were conducted to confirm the involvement of the ferroxidase site of variant A1 in iron oxidation as was previously done with HuHF and other ferritins (*4*, *20*−*23*). Figure 6 compares the kinetic traces of formation and decay of the peroxo complex in variants A1 and A2 and wild-type recombinant HuHF when 48 Fe(II) shell is added to each apoprotein sample in the presence of 21% oxygen. All three proteins exhibit peroxo complex formation, but on the basis of the intensity of the 650 nm absorbance, variant A2 produces only ∼25% as much complex as the other two proteins. Additional stopped-flow measurements with variant A2 employing Fe(II)/protein ratios from 6/1 to 48/1 revealed that the 650 nm absorbance achieves its maximum value at a ratio of only 12/1 compared to 48/1 for the other two proteins (data not shown). These results indicate that variant A2, which lacks ligand Glu61, has an impaired ability to form a peroxo complex and that on average only ∼25% of the 24 ferroxidase centers of the protein are functional under the conditions described in the legend of Figure 6.

The maximum level of formation of the peroxo complex in HuHF occurs at ∼50 ms, compared to ∼80 ms for both A1 and A2 variants (Figure 6). HuHF and variant A1 exhibit similar kinetic profiles in Figure 6 with average maximal absorbances at 650 nm of 0.114 and 0.118 [ϵ_{650} = 475 ± 3 and 492 ± 10 M^{-1} cm^{-1} per iron, respectively (N = 5), assuming 100% peroxo complex formation] and half-lives for peroxo complex decay of 1.1 and 0.91 s, respectively. The peroxo complex of variant A2 has an average maximal absorbance at 650 nm of 0.0300 [ϵ_{650} = 500 ± 6 M^{-1} cm^{-1} per iron (N = 4), corrected for 25% peroxo complex formation] and a slightly longer decay half-life of 1.3 s compared to the other two proteins.

DISCUSSION

Historically, considerable attention has been given to the identity of the residues involved in the protein-mediated fast iron oxidation process that leads to the formation of the mineral core inside the protein shell (*1*, *2*). While the secondary, tertiary, and quaternary structures of ferritins are generally conserved, few amino acid residues are highly conserved among all species (*2*, *24*). Of great importance are the ferroxidase site residues which are directly involved in the rapid oxidation and hydrolysis of iron. Substitutions of any of these conserved amino acid residues result in altered ferroxidase activities and binding stoichiometries (*4*, *5*, *12*). Recent studies have shown that either the ferrous binding stoichiometry or the kinetic behavior of the ferric core formation can be affected depending on the residue(s) that is mutated (*4*, *25*).

Because of the atypical behavior of nucleation site variant A2 (E61A/E64A/E67A) and its iron binding stoichiometry

and ferroxidase activity, which are reduced compared to those of wild-type HuHF, it was concluded that a significant structural change has occurred at the ferroxidase center of this variant (*4*, *5*). This finding is confirmed by the stopped-flow data presented here where only a limited amount of the peroxo complex is formed with variant A2 (Figure 6). In contrast to variant A2 with a previously shown binding stoichiometry of 24 Fe(III) protein (*4*), variant A1 (E64A/E67A) of this work shows a binding stoichiometry of 48 Fe(III) protein (2 Fe^{3+} ferroxidase site) and, except for a slightly slower rate of peroxo complex formation, kinetic profiles similar to those of wild-type HuHF (Figures 3−6). These results indicate that the molecular engineering of the new variant A1 did not disrupt or appreciably affect the functional properties of the protein.

The Fe(II)/O_2 stoichiometry of 2/1 obtained from oximetry measurements (Figure 2) is in accord with H_2O_2 being a product of iron oxidation, as expected for a protein-mediated ferroxidation reaction (*4*, *15*, *26*). Interestingly, the oxidation stoichiometric ratio in variant A1 reaches a plateau value of 2.9 ± 0.1 Fe(II) O_2 between 96 and 250 Fe(II) shell added (Figure 2, inset). The sharp increase in the observed Fe(II)/O_2 stoichiometry beyond 250 Fe(II) atoms/protein indicates that the mineralization reaction in which Fe(II) is oxidized by O_2 with a stoichiometry of 4/1 starts to take over as previously demonstrated for HuHF (*4*). In variant A1, an incipient core of ∼250 Fe(II) shell also appears to be required for the mineralization reaction to appreciably occur. The detailed study of the different pathways by which Fe(II) is oxidized and transferred inside the cavity of HuHF has been described elsewhere (*4*), and variant A1 seems to follow similar pathways of iron oxidation. The fact that the Fe(II)/O_2 stoichiometry does not reach the expected value of 4/1, even at high iron loadings [1000 Fe(II) shell], suggests that partially reduced oxygen species are probably released into the bulk solution due to incomplete reduction of O_2 to H_2O.

That the rates of iron oxidation measured at 305 nm are the same in both A1 and HuHF, when large amounts of Fe(II) are added (300 or 1000 Fe protein), precludes the possible involvement of nucleation site residues Glu64 and Glu67 in the mineralization reaction (Figure 5). Also, the somewhat faster apparent turnover of Fe at the ferroxidase site of variant A1 is the opposite of what is expected if Glu61 facilitates transfer of Fe(III) from the ferroxidase center to nucleation site residues Glu64 and Glu67 as previously proposed (*11*). Consistent with this observation, Mössbauer studies have shown that ∼60−80% of the 48 Fe(II) added to HuHF remained as Fe(III) oxo dimers with only 20−40% in the form of clusters when the protein was allowed to stand for 2−10 min (*27*, *28*). Even after reaction for 24 h, 13% of the added iron remained as iron(III) dimers (*28*). Other studies of iron incorporation in HuHF and its variants also showed the presence of various percentages of iron species (i.e., monomers, dimers, and clusters) at different times, pHs, and ratios of iron to protein, indicating again that the protein never clears iron completely from its ferroxidase center (*29*−*31*), consistent with only partial recovery of its ferroxidase activity as reported here (see Results).

Stopped-flow measurements on different fast oxidizing human, bacterial, and bullfrog ferritins (*20*, *22*, *23*) show a transient blue peroxodiiron(III) intermediate with a maximum absorbance λ_{max} at ∼650 nm, suggesting a common initial step for the ferroxidation reaction in all these proteins. The rapid formation of the peroxo intermediate in HuHF followed by its decay is also a feature of variant A1 (E64A/E67A) (Figure 6). Thus, except for its somewhat faster recovery of ferroxidase activity and the slightly slower rate of peroxo formation, variant A1 lacking the putative nucleation site is strikingly similar to HuHF in its mechanism of iron oxidation and mineralization at all levels of iron loading of the protein.

In conclusion, this work has shown that the putative nucleation site is not required for formation of the mineral core in H-chain ferritins as previously thought. The somewhat faster turnover of ferroxidase site iron observed here with variant A1 compared to that with HuHF suggests that residues Glu64 and Glu67 may function to retard iron clearance from the ferroxidase center, perhaps conferring a physiological advantage to the wild-type protein. This observation might explain why the two residues are highly conserved in ferritins from animals and plants (*2*). The rates of iron turnover in the C-site variants of bacterial ferritin, EcFtnA, also exceed those of the wild-type protein, suggesting that the negatively charged residues of the C-site retard the clearance of iron from the ferroxidase center of this ferritin (*32*). Thus, it is possible that the C-site of HuHF, as for EcFtnA, helps the ferroxidase site retain Fe(III) longer, keeping it in a more bioavailable form for use by the cell (*32*).

ACKNOWLEDGMENT

We thank Ms. Christine Janus-Chandler for isolating and purifying variant A1 used in this study.

REFERENCES

1. Chasteen, N. D. (1998) Ferritin. Uptake, storage, and release of iron, in *Metal Ions in Biological Systems* (Sigel, H., and Sigel, A., Eds.) Vol. 35, pp 479−514, Marcel Dekker, New York.
2. Harrison, P. M., and Arosio, P. (1996) Ferritins: molecular properties, iron storage function and cellular regulation, *Biochim. Biophys. Acta 1275*, 161−203.
3. Cowley, J. M., Janney, D. E., Gerkin, R. C., and Buseck, P. R. (2000) The structure of ferritin cores determined by electron nanodiffraction, *J. Struct. Biol. 131*, 210−216.
4. Zhao, G., Bou-Abdallah, F., Arosio, P., Levi, S., Janus-Chandler, C., and Chasteen, N. D. (2003) Multiple pathways for mineral core formation in mammalian apoferritin. The role of hydrogen peroxide, *Biochemistry 42*, 3142−3150.
5. Santambrogio, P., Levi, S., Cozzi, A., Corsi, B., and Arosio, P. (1996) Evidence that the specificity of iron incorporation into homopolymers of human ferritin L- and H-chains is conferred by the nucleation and ferroxidase centres, *Biochem. J. 314*, 139−144.
6. Crichton, R. R., Herbas, A., Chavez-Alba, O., and Roland, F. (1996) Identification of catalytic residues involved in iron uptake by L-chain ferritins, *J. Biol. Inorg. Chem. 1*, 567−574.
7. Wade, V. J., Levi, S., Arosio, P., Treffry, A., Harrison, P. M., and Mann, S. (1991) Influence of site-directed modifications on the formation of iron cores in ferritin, *J. Mol. Biol. 221*, 1443−1452.
8. Bauminger, E. R., Treffry, A., Hudson, A. J., Hechel, D., Hodson, N. W., Andrews, S. C., Levi, S., Nowik, I., Arosio, P., Guest, J. R., and Harrison, P. M. (1994) Iron incorporation into ferritins: evidence for the transfer of monomeric Fe(III) between ferritin molecules and for the formation of an unusual mineral in the ferritin of *Escherichia coli*, *Biochem. J. 302*, 813−820.
9. Santambrogio, P., Levi, S., Arosio, P., Palagi, L., Vecchio, G., Lawson, D. M., Yewdall, S. J., Artymiuk, P. J., Harrison, P. M., Jappelli, R., and Cesareni, G. (1992) Evidence that a salt bridge in the light chain contributes to the physical stability difference between heavy and light human ferritins, *J. Biol. Chem. 267*, 14077−14083.

10. Gallois, B., Langlois d'Estaintot, B., Michaux, M.-A., Dautant, A., Granier, T., Précigoux, G., Soruco, J.-A., Roland, F., Chavas-Alba, O., Herbas, A., and Crichton, R. R. (1997) X-ray structure of recombinant horse L-chain apoferritin at 2.0 Å resolution: implications for stability and function, *J. Biol. Inorg. Chem. 2*, 360−367.
11. Lawson, D. M., Artymiuk, P. J., Yewdall, S. J., Smith, J. M. A., Livingstone, J. C., Treffry, A., Luzzago, A., Levi, S., Arosio, P., Cesareni, G., Thomas, C. D., Shaw, W. V., and Harrison, P. M. (1991) Solving the structure of human H ferritin by genetically engineering intermolecular crystal contacts, *Nature 349*, 541−544.
12. Levi, S., Yewdall, S. J., Harrison, P. M., Santambrogio, P., Cozzi, A., Rovida, E., Albertini, A., and Arosio, P. (1992) Evidence of H- and L-chains have co-operative roles in the iron-uptake mechanism of human ferritin, *Biochem. J. 288*, 591−596.
13. Levi, S., Santambrogio, P., Cozzi, A., Rovida, E., Corsi, B., Tamborini, E., Spada, S., Albertini, A., and Arosio, P. (1994) The role of the L-chain in ferritin iron incorporation. Studies of homo- and heteropolymers, *J. Mol. Biol. 238*, 649−654.
14. Santambrogio, P., Cozzi, A., Levi, S., Rovida, E., Magni, F., Albertini, A., and Arosio, P. (2000) Functional and immunological analysis of recombinant mouse H- and L-ferritins from *Escherichia coli*, *Protein Expression Purif. 19*, 212−218.
15. Yang, X., Chen-Barrett, Y., Arosio, P., and Chasteen, N. D. (1998) Reaction paths of iron oxidation and hydrolysis in horse spleen and recombinant human ferritins, *Biochemistry 37*, 9743−9750.
16. Zhao, G., Bou-Abdallah, F., Yang, X., Arosio, P., and Chasteen, N. D. (2001) Is hydrogen peroxide produced during iron(II) oxidation in mammalian apoferritins? *Biochemistry 40*, 10832−10838.
17. Yang, X., Le Brun, N. E., Thomson, A. J., Moore, G. R., and Chasteen, N. D. (2000) The iron oxidation and hydrolysis chemistry of *Escherichia coli* bacterioferritin, *Biochemistry 39*, 4915−4923.
18. Jameson, G. N. L., Jin, W., Krebs, C., Perreira, A. S., Tavares, P., Liu, X., Theil, E. C., and Huynh, B. H. (2002) Stoichiometric production of hydrogen peroxide and parallel formation of ferric multimers through decay of the diferric-peroxo complex, the first detectable intermediate in ferritin mineralization, *Biochemistry 41*, 13435−13443.
19. Bou-Abdallah, F., Lewin, A. C., Le Brun, N. E., Moore, G. R., and Chasteen, N. D. (2002) Iron detoxification properties of *Escherichia coli* bacterioferritin. Attenuation of oxyradical chemistry, *J. Biol. Chem. 277*, 37064−37069.
20. Treffry, A., Zhao, Z., Quail, M. A., Guest, J. R., and Harrison, P. M. (1995) Iron(II) oxidation by H-chain ferritin: evidence from site-directed mutagenesis that a transient blue species is formed at the dinuclear iron center, *Biochemistry 34*, 15204−15213.
21. Fetter, J., Cohen, J., Danger, D., Loehr, J. S., and Theil, E. C. (1997) The influence of conserved tyrosine 30 and tissue-dependent differences in sequence on ferritin function: use of blue and purple Fe(III) species as reporters of ferroxidation, *J. Biol. Inorg. Chem. 2*, 652−661.
22. Zhao, Z., Treffry, A., Quail, M. A., Guest, J. R., and Harrison, P. M. (1997) Catalytic iron(II) oxidation in the non-heme ferritin of *Escherichia coli*: the early intermediate is not an iron tyrosinate, *J. Chem. Soc., Dalton Trans.*, 3977−3978.
23. Pereira, A. S., Small, W., Krebs, C., Tavares, P., Edmondson, D. E., Theil, E. C., and Huynh, B. H. (1998) Direct spectroscopic and kinetic evidence for the involvement of a peroxodiferric intermediate during the ferroxidase reaction in fast ferritin mineralization, *Biochemistry 37*, 9871−9876.
24. Chasteen, N. D., and Harrison, P. M. (1999) Mineralization in ferritin: an efficient means of iron storage, *J. Struct. Biol. 126*, 182−194.
25. Bou-Abdallah, F., Arosio, P., Santambrogio, P., Yang, X., Janus-Chandler, C., and Chasteen, N. D. (2002) Ferrous ion binding to recombinant human H-chain ferritin. An isothermal titration calorimetry study, *Biochemistry 41*, 11184−11191.
26. Sun, S., Arosio, P., Levi, S., and Chasteen, N. D. (1993) Ferroxidase kinetics of human liver apoferritin, recombinant H-chain apoferritin, and site-directed mutants, *Biochemistry 32*, 9362−9369.
27. Bou-Abdallah, F., Papaefthymiou, G. C., Scheswohl, D. M., Stanga, S. D., Arosio, P., and Chasteen, N. D. (2002) μ-1,2-Peroxobridged di-iron(III) dimer formation in human H-chain ferritin, *Biochem. J. 364*, 57−63.
28. Treffry, A., Hawkins, C., Williams, J. M., Guest, J. R., and Harrison, P. M. (1996) Lability of iron at the dinuclear centers of ferritin studied by competition with four chelators, *J. Biol. Inorg. Chem. 1*, 49−60.
29. Bauminger, E. R., Harrison, P. M., Hechel, D., Hodson, N. W., Nowik, I., Treffry, A., and Yewdall, S. J. (1993) Iron(II) oxidation and early intermediates of iron-core formation in recombinant human H-chain ferritin, *Biochem. J. 296*, 709−719.
30. Bauminger, E. R., Harrison, P. M., Hechel, D., Nowik, I., and Treffry, A. (1994) How does the ferritin core form? *Hyperfine Interact. 91*, 835−839.
31. Bauminger, E. R., Harrison, P. M., Hechel, D., Nowik, I., and Treffry, A. (1991) Mössbauer spectroscopic investigation of structure−function relations in ferritins, *Biochim. Biophys. Acta 1118*, 48−58.
32. Treffry, A., Zhao, Z., Quail, M. A., Guest, J. R., and Harrison, P. M. (1998) How the presence of three iron binding sites affects the iron storage function of the ferritin (EcFtnA) of *Escherichia coli*, *FEBS Lett. 432*, 213−218.

BI0498813